ADVANCED FUNCTIONAL MATERIALS
www.afm-journal.de

N-Doped Graphene-SnO_2 Sandwich Paper for High-Performance Lithium-Ion Batteries

Xi Wang, Xinqiang Cao, Laure Bourgeois, Hasigaowa Guan, Shimou Chen, Yeteng Zhong, Dai-Ming Tang, Huiqiao Li,* Tianyou Zhai,* Liang Li, Yoshio Bando, and Dmitri Golberg*

A new facile route to fabricate N-doped graphene-SnO_2 sandwich papers is developed. The 7,7,8,8-tetracyanoquinodimethane anion ($TCNQ^-$) plays a key role for the formation of such structures as it acts as both the nitrogen source and complexing agent. If used in lithium-ion batteries (LIBs), the material exhibits a large capacity, high rate capability, and excellent cycling stability. The superior electrochemical performance of this novel material is the result from its unique features: excellent electronic conductivity related to the sandwich structure, short transportation length for both lithium ions and electrons, and elastomeric space to accommodate volume changes upon Li insertion/extraction.

1. Introduction

As one of the most important energy-storage devices,[1–9] lithium-ion batteries (LIBs) have attracted much attention in the scientific and industrial fields.[10–15] There is an increasing interest in developing high-power anode materials for the next generation of high-performance rechargeable LIBs.[16–26] However, the practical use of these materials is greatly hindered by their pretty low electronic conductivity and large volume changes (>200%) upon Li insertion/extraction. To address these problems, fabricating carbonaceous nanocomposites, especially graphene-based hybrid anodes,[7,18,29–33] seems to be the most applicable strategy. However, there are still some limitations on the LIBs performance for these reported graphene-based hybrid anodes. For example, most of the active nanoparticles in these structures are simply decorated on the surface of graphene rather than being accommodated between the graphene sheets, making them vulnerable for being peeled-off upon cycling[34] (Figure S1, Supporting Information). Furthermore, the electronic paths in these surface-decorated electrodes are not effectively shortened as severe self-aggregation of the active nanoparticles inevitably occurs because of the high surface energy (Figure S2, Supporting Information).[35] Therefore, it is still a big challenge to further improve or optimize their electrochemical performance. To overcome these issues, it is believed that two strategies are feasible. The first is the fabrication of N-doped graphene (GN) because GN is expected to enhance the Li-battery properties, like other doped carbon forms. For example, Sun and co-workers synthesized a series of GN nanosheet anodes[36,37] with excellent cycle life and high lithium storage capability. Moreover, Cheng's group reported the synthesis of GN by using an NH_3 thermal treatment of pristine graphene and found that it exhibited ultrahigh capacity and rate performance.[38] Ajayan and coworkers also reported GN film anodes with enhanced electrochemical performance.[39] Very recently, Yu's group has fabricated N-doped graphene/ZnSe nanocomposites using a new route.[40] Nevertheless, the synthetic approaches of GN are mainly limited to chemical vapor deposition (CVD), thermal annealing of graphene oxide (GO) with NH_3, nitrogen plasma treatment of graphene, and the arc-discharge method. At the same time, the toxicity of the precursors (usually NH_3 or pyridine) used in these syntheses need also be considered. Therefore, it is still a challenge to prepare GN by a facile method.[41,42] The second strategy to enhance the electrochemical performance is to fabricate sandwich-structured graphene composite anodes. For

Dr. X. Wang, Dr. S. Chen, Dr. D.-M. Tang, Dr. T. Zhai, Dr. L. Li, Prof. Y. Bando, Prof. D. Golberg
International Center for Young Scientists (ICYS) and International Center for Materials Nanoarchitectonics (MANA)
National Institute for Materials Science (NIMS)
Namiki 1-1, Tsukuba, Ibaraki 305-0044, Japan
E-mail: Wang.Xi2@nims.go.jp; zhai.tianyou@gmail.com
Dr. X. Cao, Dr. Y. Zhong
Beijing National Laboratory for Molecular Science
Key Laboratory of Photochemistry
Institute of Chemistry
Chinese Academy of Sciences
Beijing 100190, P. R. China
Dr. L. Bourgeois
Monash Centre for Electron Microscopy and Department of Materials Engineering
Monash University
VIC 3800, Australia
H. Guan
Key Laboratory of Marine Chemistry Theory and Technology
Ministry of Education
Ocean University of China
Qingdao 266100, P. R. China
Dr. H. Li
Energy Technology Research Institute
National Institute of Advanced Industry and Technology (AIST)
Umezono, 1-1-1, Tsukuba, 305-8568 Japan
E-mail: Huiqiaoli@gmail.com

DOI: 10.1002/adfm.201103110

example, Zhang's group[43] prepared a multilayer nanoassembly of Sn-nanopillar arrays sandwiched between graphene layers using a conventional film deposition and annealing process, and these materials showed a high reversible capacity and excellent cycling performance even at a high current density. Furthermore, Feng and Müllen[44] have demonstrated the efficient fabrication of sandwich-like, graphene-based titania nanosheet anodes, which exhibit superior electrochemical performance in terms of their specific capacity, rate capability, and cyclability. As both strategies, either using GN or a sandwich-like graphene composite, result in improved electrochemical performances, there is a great surge in developing graphene-based composites that combine both the N-doped property and sandwich structure. However, to the best of our knowledge, little research has been done on N-doped sandwich graphene hybrid anodes up to now.

In this paper, we selected SnO_2 as the research object because of its low intercalation potential for lithium ions and high theoretical capacity (782 mAh g^{-1}),[45–47] and developed a facile strategy to fabricate N-doped graphene-SnO_2 (G-SnO_2) sandwich papers in which most of the SnO_2 nanoparticles (32 wt%) are sandwiched between the graphene layers. Here, 7,7,8,8-tetracyanoquinodimethane ($TCNQ^-$) ions play a key role in the formation of such N-doped sandwich structures, as they act both as the nitrogen source and the complexing agent. The sandwich structure not only assures solid contact between the SnO_2 particle and the graphene layer, it also facilitates a high electrode conductivity, and renders the elastomeric space needed to accommodate the volume changes of SnO_2, thus leading to an excellent electrochemical performance as the anode for lithium-ion batteries.

2. Results and Discussion

The graphene used for this work was synthesized prior to the fabrication of N-doped G-SnO_2 sandwich papers.[30] Atomic force microscopy (AFM), high-resolution transmission electron microscopy (HRTEM), and X-ray photoelectron spectroscopy (XPS) data (**Figure 1**, Figure S3, Supporting Information) verified the high quality of the obtained graphene (G). N-doped G-SnO_2 papers were fabricated via a three-step route (**Scheme 1**): first, $TCNQ^-$, evidenced by UV-vis spectroscopy (**Figure 2**),[48] was absorbed on the surface of graphene, after which the negatively charged G easily dispersed in the solvent to form a homogeneous suspension,[49] as the electrostatic repellency effectively prevents the inter- or intra- π–π stacking of graphene (step 1). After careful addition of the Sn^{II} salt, the G layers containing Sn-TCNQ self-assemble into a sandwich because of the strong electrostatic interactions between Sn^{2+} and $TCNQ^-$ (step 2), and then precipitate from the solution due to the insolubility of Sn-TCNQ in the used solvents; this process guarantees the incorporation of Sn-TCNQ (i.e., SnO_2 in final product) between the two layers of graphene. It should be noted that the mixed organic

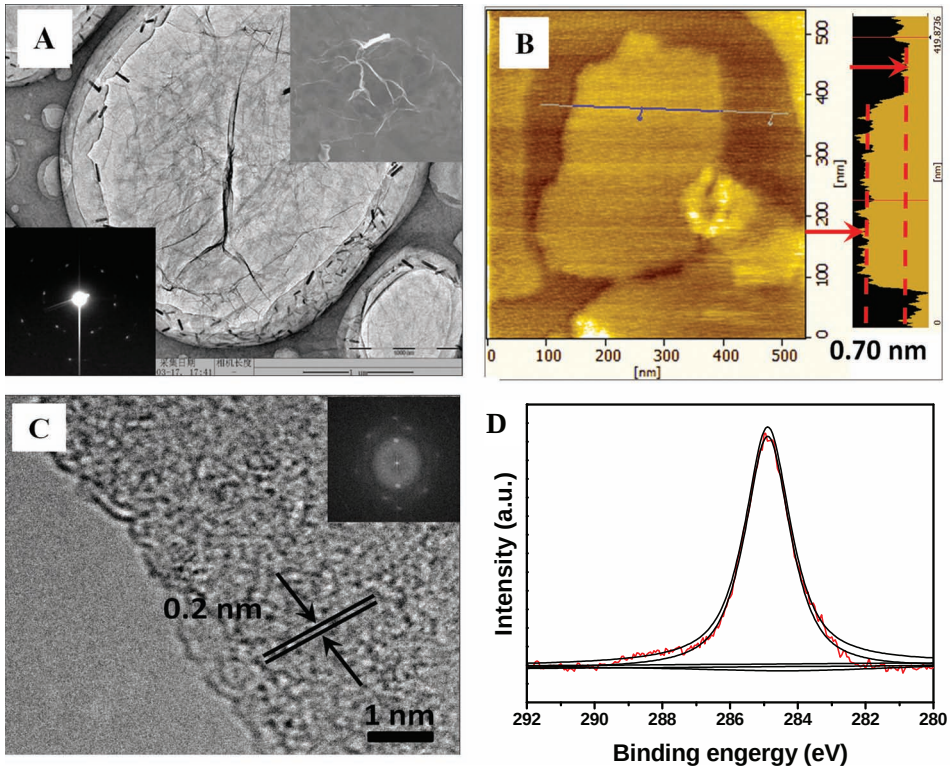

Figure 1. A) TEM image of a single graphene sheet, the insets show the FFT (bottom left) and SEM image (top right); B) AFM image and corresponding height profile of a single-layer graphene sheet; C) HRTEM image and its FFT of a graphene sheet obtained after calcinations at 800 °C. D) XPS C1s spectrum of graphene.

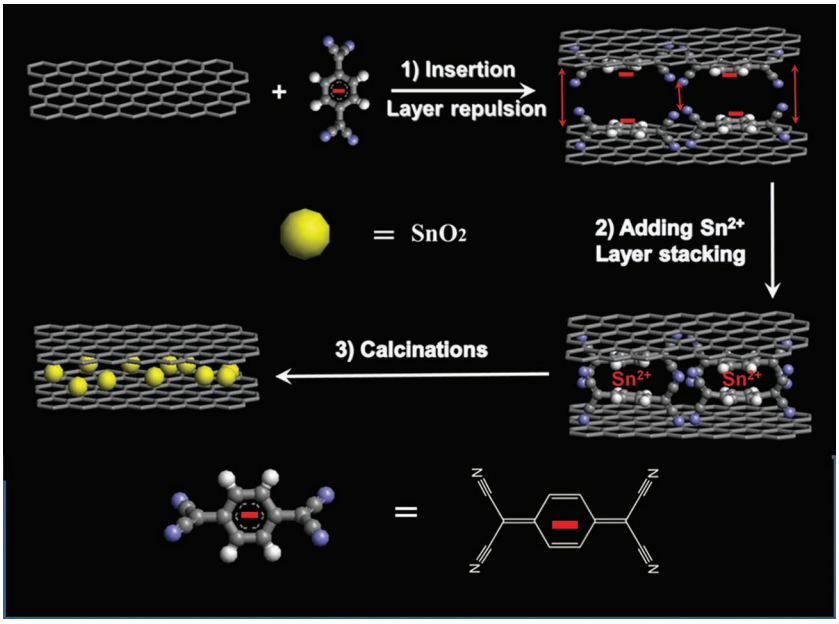

Scheme 1. Schematic illustration of the formation process of N-doped G-SnO_2 sandwich papers.

solvents play an important role in the formation of Sn-TCNQ adsorbed on graphene paper: using H_2O/*N*,*N*-dimethylformamide as a solution ensures that graphene remains suspended rather than precipitates,[50] and $TCNQ^-$ ions are formed more easily in organic solution (such as *N*,*N*-dimethylformamide and acetonitrile) than in water.[48] Finally, the obtained precipitation was dried and annealed under inert gas atmosphere to obtain the sandwich-type G-SnO_2 papers (step 3), in which the SnO_2 nanoparticles are well encapsulated between the G layers. It is worth noting that certain amounts of carbon in the graphene are also substituted by nitrogen; thus, N-doped graphene can easily be formed because $TCNQ^-$ contains four N atoms per molecule and calcination can take place in the relatively closed sandwich structures.

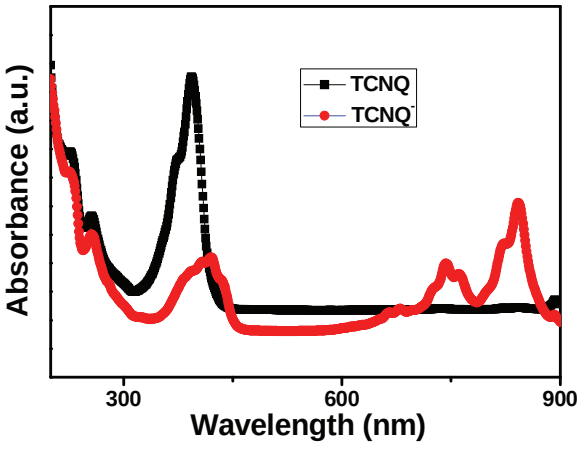

Figure 2. UV-vis spectra of TCNQ (black line) and $TCNQ^-$ (red line) dispersed in an acetonitrile solution.

A scanning electron microscopy (SEM) image of the cross section of such a N-doped G-SnO_2 fractured paper sample exhibited a layered structure (**Figure 3**A). Its composition was confirmed by X-ray diffraction (XRD) (Figure 3B). The broad diffraction peak observed at around 23° (3.85 Å) is close to but certainly larger than the d_{002}-spacing of graphite (3.35 Å), and also larger than that commonly obtained for G paper (24°, approximately 3.70 Å) dried in the same way at 150 °C.[50] This indicates the existence of an interlayer of SnO_2 nanoparticles, which leads to the relatively less dense packing of the G sheets (larger interlayer distance between sheets) than is the case for pure G upon drying.[30] The sandwich structures can also be partly shown by relating Raman spectra (**Figure 4**) of the N-doped G-SnO_2 samples with those of pure graphene papers. Compared to pure G paper, the G-band in G-SnO_2 paper is slightly shifted which may be attributed to the existence of SnO_2 between the graphene layers.[51] The average SnO_2 particle size estimated from the (110) peak according to the Scherrer equation is 3.7 nm, which is close to that observed from the high-resolution (HR)TEM images (Figure 3C). From the HRTEM image of a single nanoparticle (**Figure 5**), the observed lattice fringes are consistent with the SnO_2 phase ($P4_2/mnm$, a = 4.74 Å, c = 3.19 Å) viewed along [001]. From these images (Figure 3C, Figure S4, upper part, Supporting Information), the ordered crystal lattices of the SnO_2 nanoparticles and the curved layers of graphene can clearly be seen, further confirming the dispersion of SnO_2 nanoparticles between the graphene layers. It should be noted that some elongated 1D nanocrystals (Figure 3C, Figure S4, lower part, Supporting Information) were also found, which certifies the space-confining effect of two neighboring graphene layers. The interlayer space of graphene can act as a nanoscale reactor, which effectively restricts the growth of the SnO_2 nanoparticles and further drives the fusion of two or more nanoparticles into a 1D nanostructure within the lamellar superstructure. It should also be noted that most particles are epitaxially fused together towards [110] because of the continuity of the lattice (110) planes across the interface (Figure 3C), indicating that the oriented attachments occur along the {110} facets. To the best of our knowledge, this is the first observation of such 1D nanocrystals between graphene layers. This finding may provide a novel approach to synthesize ultra-thin 1D or even 2D nanostructures.

To provide more proof of the sandwich structure, we carried out additional experiments. We used the method reported by Guo[52] to synthesize SnO_2/graphene composites that have a near monolayer dispersion of SnO_2 nanocrystals on both sides of the graphene, which results in a high SnO_2 content of over 32 wt%. Then, a controlled etching experiment was carried out on both this sample and our sandwich-type G-SnO_2 sample. After dispersing the same amount of our sample and of the SnO_2/graphene composite into equal volumes of diluted

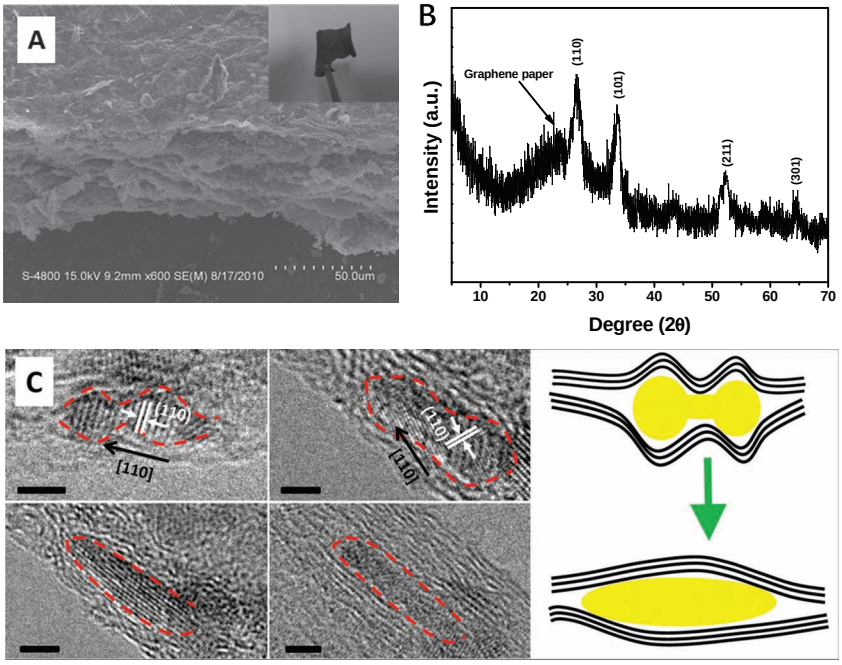

Figure 3. A) Cross-sectional SEM image of G-SnO_2 paper, the inset shows the real product appearance. B) XRD pattern of G-SnO_2 papers. C) Different modes of SnO_2 particles existing between the layers of graphene and their schematic description, scale bar: 1 nm.

HCl solution for a certain time we tested the changes in the two samples by XRD and TEM, as shown in the Supporting Information (Figures S5, S6). For the SnO_2/graphene composites, the typical peaks (Figure S5A) in the XRD pattern widened and their intensity decreased after immersion in HCl. From the TEM observation (Figure S6A-B), we can also see that both the SnO_2 amount and the particle size decreased much by the HCl etching. These observations indicate that most of the SnO_2 nanoparticles in this composite sample are easily etched away by immersion in diluted HCl. In contrast, there is little change in the XRD pattern (Figure S5B) of our sample before and after HCl etching. TEM images of our sandwich-type G-SnO_2 sample (Figure S6C-D) also showed that most of the SnO_2 nanoparticles are left on the sample and remain located between the graphene layers.

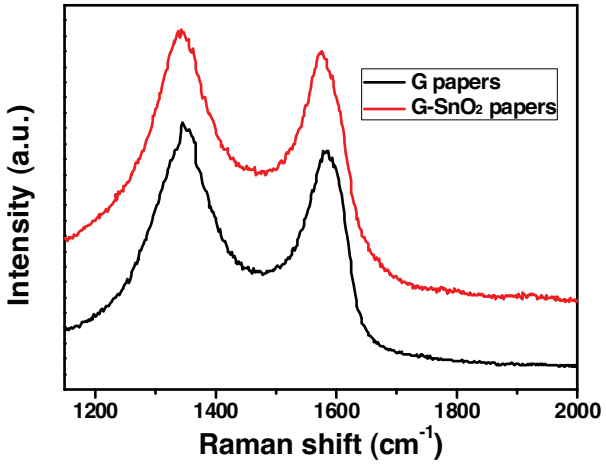

Figure 4. Raman spectra of graphene (G) papers and N-doped G-SnO_2 papers.

In order to investigate the distribution and composition of the surface layer of N-doped G-SnO_2 papers, energy-dispersive X-ray (EDX) mapping analysis and X-ray photoemission spectroscopy (XPS) were carried out. The EDX mapping images of Sn, C, and N are shown in **Figure 6**. From these images, one can see that a large amount of Sn and N elements are included in the hybrids and the distribution of the Sn and N elements is wide and even includes the graphene region. The XPS survey spectra of our N-doped G-SnO_2 papers (**Figure 7**) indicate the presence of the principal C1s, O1s, and N1s core levels. The atomic percentage of doped nitrogen is about 8%, which is comparable to that obtained by using a traditional ammonia-mediated CVD method.[53] The above analysis verifies that our method is an effective strategy to synthesize N-doped graphene. As shown in Figure 7B, the peak of the C1s core-level spectrum can be fitted with three components: the main peak at a binding energy of 284.6 eV can be assigned to sp^2 hybridized C atoms in graphene, whereas the other two peaks, located at 285.5 eV and 287.1 eV, should be assigned to sp^2 C and sp^3 C atoms bonded to N, respectively.[39] Similarly, the N1s peak can also be resolved into three components centered at 399.1, 400.2, and 401.8 eV, representing pyridinic, pyrrolic, and graphitic type of N atoms doped in the graphene structure, respectively (Figure 7C). In addition, the Sn $3d_{5/2}$ (487.3 eV) and Sn $3d_{3/2}$ (495.8 eV) peaks found in the XPS data (Figure 7D) further confirm the formation of SnO_2. Both the EDX and XPS data verify that the weight percentage of SnO_2 in the final products is about 32%. This value further proves that this new route indeed can be used to fabricate sandwich-type structure papers with high SnO_2 content, because such sandwich-type graphene papers could also have been obtained but with a low amount of SnO_2 if the graphene-SnO_2 was simply filtrated from the graphene containing solution.[7]

The electrochemical performance of the N-doped G-SnO_2 paper was evaluated for Li insertion/extraction in comparison to that of commercial SnO_2 nanoparticles (20–50 nm) by using 1 M $LiClO_4$ in ethyl carbonate/diethyl carbonate (EC/DEC) as the electrolyte. A voltage plateau at 0.8 V was observed for both the commercial SnO_2 nanoparticles and our G-SnO_2 papers (**Figure 8**) at the first discharge step, indicative of the typical voltage trend of SnO_2, whereas G papers without SnO_2 showed no obvious voltage plateau during the intercalation of Li^+. At the second discharge, the N-doped G-SnO_2 paper delivered a capacity of 918 mAh g^{-1}, which is higher than those obtained for both pure SnO_2 nanoparticles (881 mAh g^{-1}) and G paper (548 mAg h^{-1}) (Figure 8). More importantly, our N-doped G-SnO_2 papers exhibited much enhanced rate capacities, as shown in **Figure 9**A. The specific capacity was maintained at

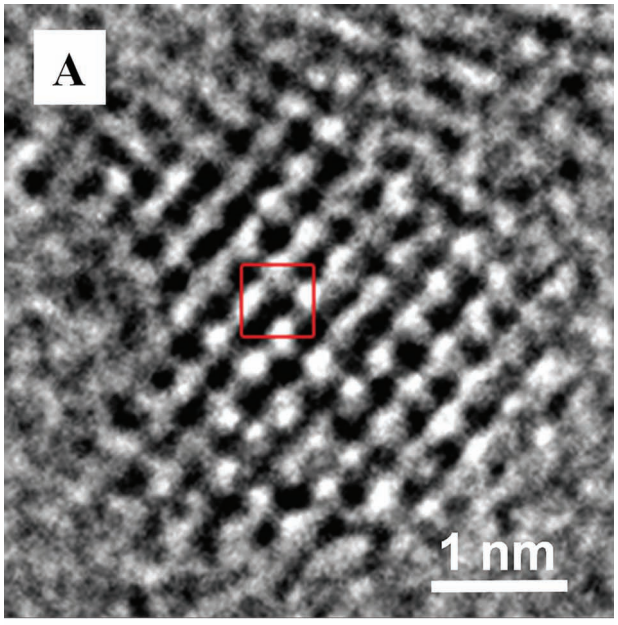

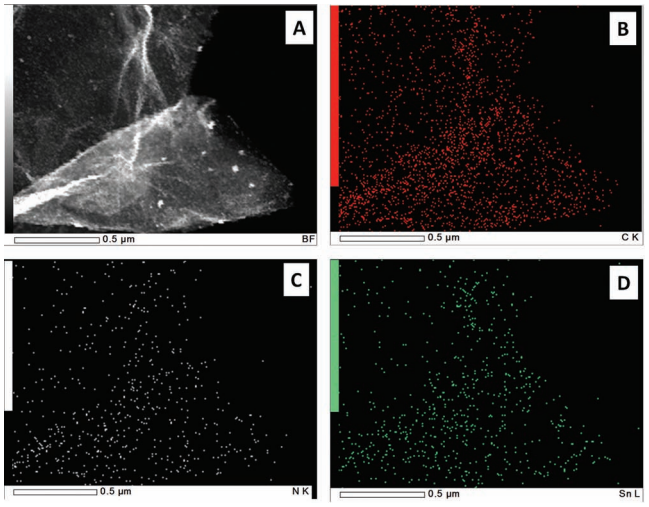

Figure 6. A) SEM image of N-doped G-SnO_2 hybrids obtained after ultrasonic treatment, B-D) the corresponding EDX mapping images of C (B), N (C), and Sn (D) elements.

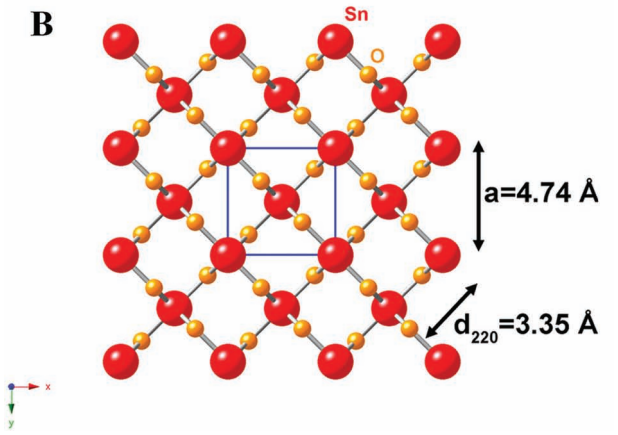

Figure 5. A) HRTEM image of a single SnO_2 nanoparticle taken from N-doped G-SnO_2 papers. B) The corresponding schematic atomic model of the SnO_2 nanoparticle from top view. It shows that the particle has lattice fringes consistent with SnO_2 viewed down [001] with the crystal structure of $P4_2/mnm$, $a = 4.74$ Å, $c = 3.19$ Å.

values as high as 683 mAh g^{-1} and 619 mAh g^{-1} after the current density was increased to 1000 mA g^{-1} and 2000 mA g^{-1}, respectively. Even at a current density of 5000 mA g^{-1}, our material still delivered a capacity of 504 mAh g^{-1}, which is 1.35 times the theoretical capacity of graphite (372 mAh g^{-1}). As for the commercial SnO_2 nanoparticles (Figure 9B), their capacity rapidly decayed from 894 mAh g^{-1} at a current density of 50 mA g^{-1} to 153 mAh g^{-1} at 1000 mA g^{-1}, and to 12 mAh g^{-1} at 2000 mA g^{-1}. Figure 9C,D shows the cyclic performances of N-doped G-SnO_2 papers and pure SnO_2 nanoparticles, respectively, at a current density of 50 mA g^{-1}. It is clear that the cycling performance of N-doped G-SnO_2 is much better than that of the SnO_2 particles. After the 1st cycle N-doped G-SnO_2 maintains the reversible capacity well and shows about 63% retention (910 mAh g^{-1}) of the initial capacity after 50 cycles, leading to an ultralow 0.02% capacity loss per cycle; whereas the SnO_2 nanoparticles exhibit a fast reversible capacity loss and only 7% retention (117 mAh g^{-1}) even after only 30 cycles, resulting in 2.9% capacity loss per cycle. In addition, the Coulombic efficiency of the N-doped G-SnO_2 paper rapidly increases to nearly 100% (inset, Figure 9C) after the first cycle, indicating very good reversibility. For comparison, we also used the method reported by Guo[52] to synthesize SnO_2/graphene composites with a high SnO_2 content (over 32 wt%) and measured their electrochemical performance (Figure S7, Supporting Information). It is can clearly be seen that our G-SnO_2 papers exhibit a much better cycling performance and enhanced rate capacities than the SnO_2/graphene composites. As shown in Figure S7, the SnO_2/graphene composites exhibit an initial reversible capacity of 1300 mAh g^{-1}, with 45% retention of the initial capacity (583 mAh g^{-1}) after 20 cycles, leading to a 2.7% capacity loss per cycle compared to the ultralow 0.02% capacity loss per cycle for our G-SnO_2 papers. As for the rate performance, the capacity of the SnO_2/graphene composites rapidly decayed from 1300 mAh g^{-1} at a current density of 50 mA g^{-1} to 245 mAh g^{-1} at 1000 mA g^{-1}, and to 112 mAh g^{-1} at 2000 mA g^{-1}. These values are much lower than that of our G-SnO_2 papers even at the high current density of 5000 mA g^{-1} (504 mAh g^{-1}). It is evident that our N-doped G-SnO_2 sandwich hybrids have a much enhanced performance over commercial SnO_2 particles and over previously reported graphene/SnO_2 composites. This shows that the N-doped G-SnO_2 sandwich structure is indeed a promising strategy to improve the electrochemical performance of G-SnO_2 hybrids. In addition, we also measured the electrochemical performance of G-SnO_2 papers over 100 cycles, as showing in Figure S8. During the 100 cycles, the N-doped G-SnO_2 paper still maintained its reversible capacity well. The cycling performance of the G-SnO_2 paper does not change a lot if extending the cycle number from 50 to 100. The capacity loss between the 51st and 100th cycle is about 0.3%, which is similar to that between the

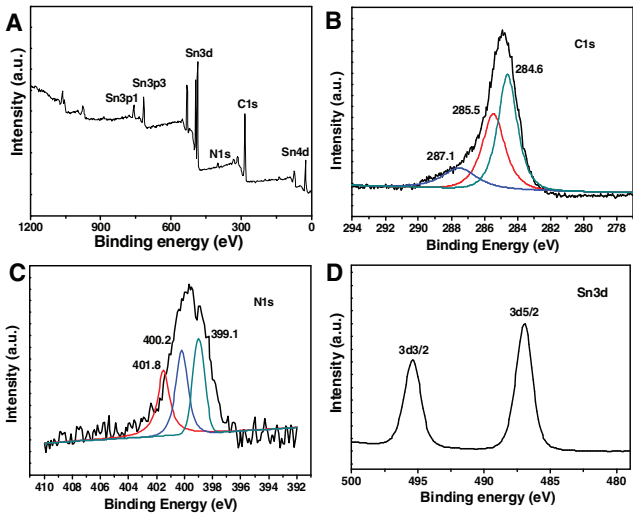

Figure 7. A) XPS survey spectra of N-doped G-SnO_2 papers. B) XPS C1s spectrum, which can be split in to two Lorentzian peaks at 284.6, 285.5 and 287.1 eV, C) XPS N1s spectrum, and D) XPS Sn3d spectrum.

second and 50th cycle (0.1%). So, we think our N-doped G-SnO_2 sandwich hybrids show a quite stable cycle performance especially compared to pure SnO_2.

Such superior electrochemical performances are believed to result from the unique features of the N-doped G-SnO_2 paper, as shown in Figure 9E. Firstly, N-doped graphene may favor a larger reversible capacity over pristine graphene as a large number of surface defects are introduced onto the graphene by N-doping.[37–39] The presence of pyridinic N atoms has been reported to lead to a disordered carbon structure which can accommodate higher amounts of Li^+, and, thus, improves the reversible capacity of the N-doped graphene electrode compared to pristine graphene electrodes. Secondly, the conductivity of the N-doped G-SnO_2 sandwich papers is dramatically enhanced (here, five times) compared to that of normal SnO_2/carbon composites. In the sandwich structure, the electronic transport length (*Le*) in our N-doped G-SnO_2 paper is effectively shortened to a level comparable to the particle size of the nanocrystals (Figure S2B, Supporting Information and Figure 5).[35] Moreover, the graphene sheets provide a continuous conductive path between the SnO_2 nanocrystals, thus, also reducing the particle–particle interface resistance (Figure S2B, Supporting Infomration). Thirdly, a super-flexible coating made of graphene sheets covering the SnO_2 nanocrystals not only provides an elastic buffer space to accommodate the volume changes upon lithium-ion insertion/extraction, but also efficiently prevents the aggregation of the nanoparticles and the cracking or crumbling of the electrode material, and, therefore, a better cycle performance can be obtained. Even though volume expansion still happens, the electrode will not pulverize as the graphene sheets can deform resiliently to accommodate such volume changes (Figure S1B, Supporting Information). In case of the non-sandwich graphene composites, the amorphous alloy aggregates formed after lithiation[34] are easily peeled off from the surface of graphene upon cycling because of the weak contact between the particle and graphene

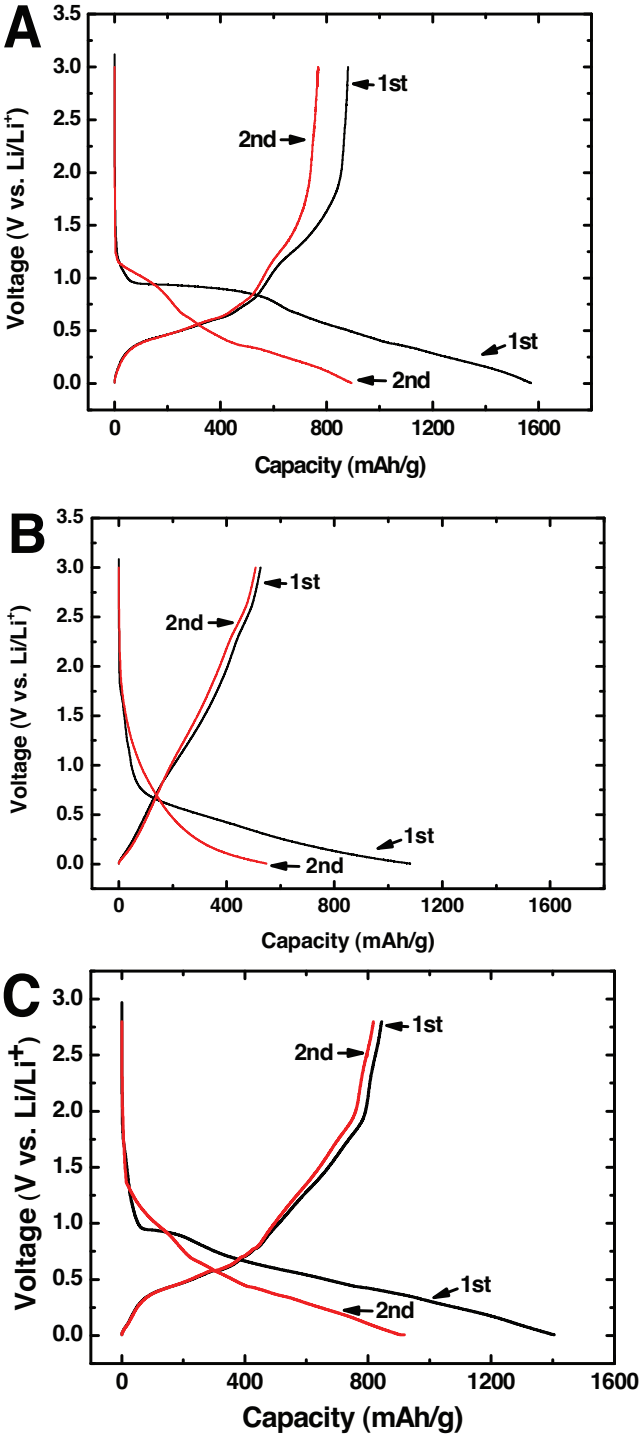

Figure 8. The first and second cycle of discharge/charge profiles for different samples: A) commercial SnO_2 nanoparticles, B) G paper, C) N-doped G-SnO_2 sandwich paper. The current density is 100 mA g^{-1}.

(Figure S1A, Supporting Information), thus leading to a fast decay of the electrode capacity. Fourthly, the loose stacking of the graphene layers enables good electrolyte penetration, giving rise to a large contact area between the active material and the electrolyte; the relatively large interlayer spacing between the

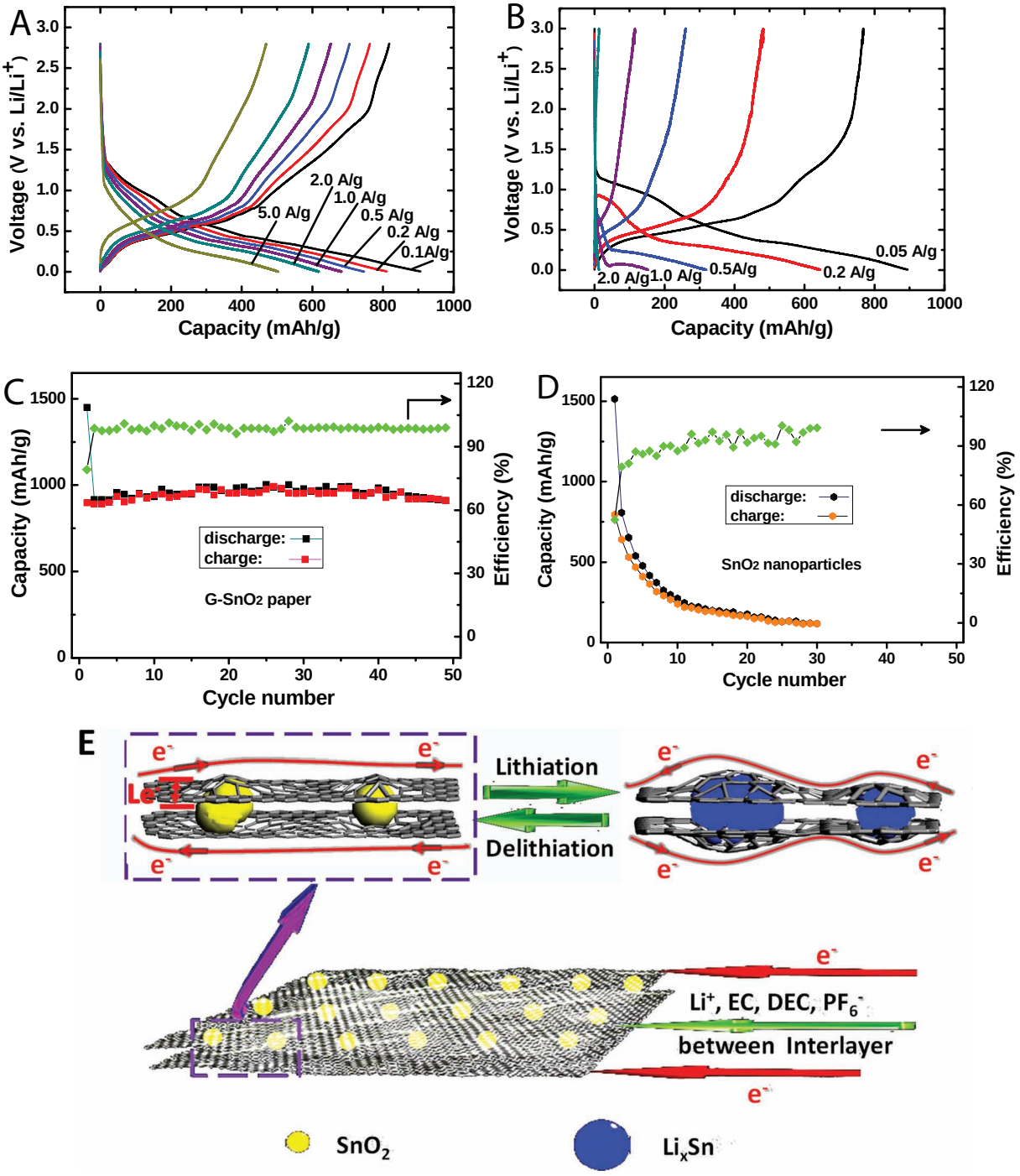

Figure 9. Charge/discharge curves of A) N-doped G-SnO_2 papers andB) commercial SnO_2 nanoparticles (20–50 nm) at various current densities. C,D)Cycling performance of N-doped G-SnO_2 paper (C) and SnO_2 nanoparticles (D) at a current density of 50 mA g^{-1}. E) Schematic representation showing paths for lithium-ions and electrons (*Le*) in the N-doped G-SnO_2 paper, respectively.

two graphene sheets provides fast and versatile transport pathways for the electrolyte ions. Moreover, the ultra-small SnO_2 nanocrystals (2–5 nm) render a very short transport length for lithium ions during insertion/extraction, which also favors a high rate charge/discharge performance. The above synergetic effects arising from the N-doped sandwich construction of conducting graphene sheets and nanosized SnO_2 filler particles is responsible for the excellent electrochemical performance of the overall electrode through the maximum utilization of the electrochemically active materials.

3. Conclusions

N-doped G-SnO_2 sandwich papers have been fabricated via a novel approach. The 7,7,8,8-tetracyanoquinodimethane anion plays a key role for the formation of such structures, as it acts as both the nitrogen source and the complexing agent. When used in LIBs, this material exhibits a very large capacity, high rate capability, and excellent cycling stability. All these notably enhanced electrochemical performances of this novel material with respect to commercial SnO_2 nanoparticles can be attributed to the structural features that provide a large number of surface defects induced onto the graphene by N-doping, excellent electronic conductivity, short transportation length for both lithium ions and electrons, and enough elastomeric space to accommodate volume changes upon Li insertion/extraction.

4. Experimental Section

Synthesis of N-doped G-SnO_2 Sandwich Papers: The graphene oxide (GO) used in this work was prepared by a modified Hummers method.[50] A homogeneous graphene oxide (30 mg) suspension was firstly prepared in 37 mL of H_2 O/*N*,*N*-dimethylformamide (DMF) solvent mixture (volume ratio DMF/H_2O = 9). Then hydrazine monohydrate (1 μL for 3 mg of GO) was added to the suspension (pH about 6.5), and the mixture was stirred at 80 °C for 12 h with N_2 flowing. A black suspension (pH about 7) of graphene (G) sheets was finally yielded. A freshly prepared green 7,7,8,8-tetracyanoquinodimethane anion ($TCNQ^-$) acetonitrile solution was added to the above graphene suspension with stirring and under N_2 flowing, after which a certain amount of $SnCl_2$ was quickly added to the solution. The obtained precipitate was washed several times by a large amount of water and ethanol and dried under vacuum at 90 °C for 12 h. The above paper-like samples were thermally treated at 800 °C for 2 h at a heating rate of 1 °C min^{-1} in a tube furnace under Ar gas flow (pressure: ca. 1 atm, rate: 100 sccm), then the furnace was cooled naturally to room temperature.

Characterizations: Transmission electron microscopy (TEM) images were taken with a JEOL F3000 microscope operated at 300 kV. The samples were first dispersed in ethanol and then collected using carbon-film-covered copper grids for analysis. Scanning electronic microscopy (SEM) images were recorded on a Hitachi S4800 electron microscope operating at 15 kV. XRD patterns were recorded on a Philips X Pert PRO MPD X-ray diffractometer operated at 35 kV and 45 mA using Cu Kα radiation. XPS measurements were carried out with an ESCALab220i-XL spectrometer using a twin-anode Al Kα (1486.6 eV) X-ray source. All spectra were calibrated to the binding energy of the C 1s peak at 284.6 eV. The base pressure was around 3×10^{-7} Pa. Raman spectra were taken on a Horiba Jobin-Yvon T6400 Raman spectrometer.

Electrochemical Tests: The electrochemical properties of N-doped G-SnO_2 papers, G papers, G-SnO_2 composites without sandwich structures, and commercial SnO_2 nanoparticles (20–50 nm) were measured using a three-electrode cell. For the testing of G-SnO_2 papers and G papers, the working electrode was prepared by directly pressing a piece of sample paper onto the Cu mesh current collector. For the testing of commercial SnO_2 nanoparticles, the working electrode was prepared by pressing the slurry of 80% SnO_2 powder, 10% acetylene black, and 10% polyvinylidene difluoride (PVDF) binder (by weight) onto the copper current collector. Li metal foil was selected as the reference and counter electrode. The electrolyte was 1 M $LiClO_4$ in ethyl carbonate (EC) and diethyl carbonate (DEC) (EC/DEC = 1:1 in v/v). The cells were assembled in a glove box filled with pure argon gas. Galvanostatic discharge/charge measurements were performed over a potential range of 3 V–0.05 V vs. Li^+/Li. Here the total weight of the N-doped G-SnO_2 paper was used to calculate the capacity values.

Supporting Information

Supporting Information is available from the Wiley Online Library or from the author. Included are schemes illustrating the morphology changes in the lithiation-delithiation process and the different electronic transport length (*Le*) of our G-SnO_2 papers and SnO_2/graphene composites; XPS of the pristine graphene oxide sheets; XRD patterns and TEM images of our G-SnO_2 papers and SnO_2/graphene composites before and after HCl treatment; discharge capacity retention over 100 cycles for the N-doped G-SnO_2 papers.

Acknowledgements

This work was supported by the Japan Society for Promotion of Science (JSPS) and the International Center for Materials Nanoarchitectonics (MANA) tenable at the National Institute for Materials Science (NIMS).

Received: December 22, 2011
Revised: January 31, 2012
Published online: April 17, 2012

[1] Z. L. Wang, J. H. Song, *Science* **2006**, *14*, 242.
[2] X. Wang, H. Guan, S. Chen, H. Li, T. Zhai, D. Tang, Y. Bando, D. Golberg, *Chem. Commun.* **2011**, *47*, 12280.
[3] J. J. Yoo, K. Balakrishnan, J. Huang, V. Meunier, B. G. Sumpter, A. Srivastava, M. Conway, A. L. M. Reddy, J. Yu, R. Vajtai, P. M. Ajayan, *Nano Lett.* **2011**, *11*, 1423.
[4] W. Gao, N. Singh, L. Song, Z. Liu, A. L. M. Reddy, L. Ci, R. Vajtai, Q. Zhang, B. Q. Wei, P. M. Ajayan, *Nat. Nanotechnol.* **2011**, *6*, 496.
[5] X. Wang, L. Yu, X. Wu, Y. Guo, F. Yuan, Y. Ma, J. Yao, *J. Phys. Chem. C* **2009**, *113*, 15553.
[6] Z. Chen, W. Ren, L. Gao, B. Liu, S. Pei, H.-M. Cheng, *Nat. Mater.* **2011**, *10*, 424.
[7] Z. S. Wu, W. C. Ren, L. Wen, L. B. Gao, J. P. Zhao, Z. P. Chen, G. M. Zhou, F. Li, H.-M. Cheng, *ACS Nano* **2010**, *4*, 3187.
[8] S. Sun, G. Zhang, D. Geng, Y. Chen, R. Li, M. Cai, X. Sun, *Angew. Chem. Int. Ed.* **2011**, *50*, 422.
[9] M.-R. Gao, Q. Gao, J. Jiang, C.-H. Cui, W.-T. Yao, S.-H. Yu, *Angew. Chem. Int. Ed.* **2011**, *50*, 4905.
[10] H. Guan, X. Wang, H. Li, C. Zhi, T. Zhai, Y. Bando, D. Golberg, *Chem. Commun.* **2012**, Doi:10.1039/c2cc30843f.
[11] J. M. Tarascon, M. Armand, *Nature* **2001**, *414*, 359.
[12] B. Dunn, H. Kamath, J. M. Tarascon, *Science* **2011**, *334*, 928.
[13] X. W. Lou, L. A. Archer, Z. C. Yang, *Adv. Mater.* **2008**, *20*, 3987.
[14] Y.-G. Guo, J.-S. Hu, L.-J. Wan, *Adv. Mater.* **2008**, *20*, 2878.
[15] P. G. Bruce, B. Scrosati, J.-M. Tarascon, *Angew. Chem. Int. Ed.* **2008**, *47*, 2930.
[16] X. Wang, X.-L. Wu, Y.-G. Guo, Y. Zhong, X. Cao, Y. Ma, J. Yao, *Adv. Funct. Mater.* **2010**, *20*, 1680.
[17] J. H. Liu, J. S. Chen, X. F. Wei, X. W. Lou, X. W. Liu, *Adv. Mater.* **2011**, *23*, 998.
[18] W. W. Zhou, J. X. Zhu, C. W. Cheng, J. P. Liu, H. P. Yang, C. X. Cong, C. Guan, X. T. Jia, H. J. Fan, Q. Y. Yan, C. M. Li, T. Yu, *Energy Environ. Sci.* **2011**, *4*, 4954.
[19] J. P. Liu, J. Jiang, C. W. Cheng, H. X. Li, J. X. Zhang, H. Gong, H. J. Fan, *Adv. Mater.* **2011**, *23*, 2076.

[20] W. W. Zhou, C. W. Cheng, J. P. Liu, Y. Y. Tay, J. Jiang, X. T. Jia, J. X. Zhang, H. Gong, H. H. Hng, T. Yu, H. J. Fan, *Adv. Funct. Mater.* **2011**, *21*, 2439.
[21] L. Hu, J. W. Choi, Y. Yang, S. Jeong, F. L. Mantia, L.-F. Cui, Y. Cui, *Proc. Natl. Acad. Sci.* **2009**, *106*, 21 490.
[22] Y. Zhong, X. Wang, K. Jiang, J. Zheng, Y. Guo, Y. Ma, J. Yao, *J. Mater. Chem.* **2011**, *21*, 17998.
[23] X. Wang, D. Tang, H. Li, W. Yi, T. Zhai, Y. Bando, D. Golberg, *Chem. Commun* **2012**, Doi: 10.1039/C2CC30643C.
[24] H. Han, T. Song, J.-Y. Bae, L. F. Nazar, H. Kim, U. Paik, *Energy Environ. Sci.* **2011**, *4*, 4532.
[25] H. Guan, X. Wang, S. Chen, Y. Bando, D. Golberg, *Chem. Commun.* **2011**, *47*, 12098.
[26] T. Song, J. Xia, J.-H. Lee, D. H. Lee, M.-S. Kwon, J.-M. Choi, J. Wu, S. K. Doo, H. Chang, W. I. Park, D. S. Zang, H. Kim, Y. Huang, K.-C. Hwang, J. A. Rogers, U. Paik, *Nano Lett.* **2010**, *10*, 1710.
[27] A. Kumar, A. L. M. Reddy, A. Mukherjee, M. Dubey, X. Zhan, N. Singh, L. Ci, W. E. Billups, J. Nagurny, G. Mital, P. M. Ajayan, *ACS Nano* **2011**, *5*, 4345.
[28] H. Gullapalli, A. L. M. Reddy, S. Kilpatrick, M. Dubey, P. M. Ajayan, *Small* **2011**, *7*, 1697.
[29] H. Wang, L. Cui, Y. Yang, H. S. Casalongue, J. T. Robinson, Y. Liang, Y. Cui, H. Dai, *J. Am. Chem. Soc.* **2010**, *132*, 13978.
[30] S. M. Paek, E. Yoo, I. Honma, *Nano Lett.* **2009**, *9*, 72.
[31] S. Yang, X. L. Feng, S. Ivanovici, K. Müllen, *Angew. Chem. Int. Ed.* **2010**, *49*, 8408.
[32] W. M. Zhang, J. S. Hu, Y. G. Guo, S. F. Zheng, L. S. Zhong, W. G. Song, L. J. Wan, *Adv. Mater.* **2008**, *20*, 1160.
[33] Y. Chen, Y. Zhang, D. Geng, R. Li, H. Hong, J. Chen, X. Sun, *Carbon* **2011**, *49*, 4434.
[34] J. Y. Huang, L. Zhong, C. M. Wang, J. P. Sullivan, W. Xu, L. Q. Zhang, S. X. Mao, N. S. Hudak, X. H. Liu, A. Subramanian, H. Fan, L. Qi, A. Kushima, J. Li, *Science* **2010**, *330*, 1515.
[35] Y. Wang, H. Li, P. He, E. Hosono, H. Zhou, *Nanoscale* **2010**, *2*, 1294.
[36] X. Li, D. Geng, Y. Zhang, X. Meng, R. Li, X. Sun, *Electrochem. Commun.* **2011**, *13*, 822.
[37] Y. Li, J. Wang, X. Li, D. Geng, R. Li, X. Sun, *Chem. Commun.* **2011**, *47*, 9438.
[38] Z.-S. Wu, W. Ren, L. Xu, F. Li, H.-M. Cheng, *ACS Nano* **2011**, *5*, 5463.
[39] A. L. M. Reddy, A. Srivastava, S. R. Gowda, H. Gullapalli, M. Dubey, P. M. Ajayan, *ACS Nano* **2010**, *4*, 6337.
[40] P. Chen, T.-Y. Xiao, H.-H. Li, J.-J. Yang, Z. Wang, H.-B. Yao, S.-H. Yu, *ACS Nano* **2012**, *6*, 712.
[41] H. M. Jeong, J. W. Lee, W. H. Shin, Y. J. Choi, H. J. Shin, J. K. Kang, J. W. Choi, *Nano Lett.* **2011**, *11*, 2472.
[42] X. L. Li, H. L. Wang, J. T. Robinson, H. Sanchez, G. Diankov, H. Dai, *J. Am. Chem. Soc.* **2009**, *131*, 15939.
[43] L. Ji, Z. Tan, T. Kuykendall, E. J. An, Y. Fu, V. Battaglia, Y. Zhang, *Energy Environ. Sci.* **2011**, *4*, 3611.
[44] S. Yang, X. Feng, K. Müllen, *Adv. Mater.* **2011**, *23*, 3575.
[45] Z. Y. Wang, D. Y. Luan, F. Y. C. Boey, X. W. Lou, *J Am. Chem. Soc.* **2011**, *133*, 4738.
[46] S. J. Ding, J. S. Chen, G. G. Qi, X. N. Duan, Z. Y. Wang, E. P. Giannelis, L. A. Archer, X. W. Lou, *J. Am. Chem. Soc.* **2011**, *133*, 21.
[47] S. Jeong, M. T. McDowell, Y. Cui, *ACS Nano* **2011**, *5*, 5800.
[48] L. R. Melby, R. J. Harder, W. R. Herteler, W. Wahler, R. E. Beson, W. E. J. Mochel, *J. Am. Chem. Soc.* **1962**, *84*, 3374.
[49] R. Hao, W. Qian, L. Zhang, Y. L. Hou, *Chem. Commun.* **2008**, 6576.
[50] S. Park, J. An, I. Jung, R. D. Piner, S. J. An, X. Li, A. Velamakanni, R. S. Ruoff, *Nano Lett.* **2009**, *9*, 1593.
[51] T. M. G. Mohiuddin, A. Lombardo, R. R. Nair, A. Bonetti, G. Savini, R. Jalil, N. Bonini, D. M. Basko, C. Galiotis, N. Marzari, K. S. Novoselov, A. K. Geim, A. C. Ferrari, *Phys. Rev. B* **2009**, *79*, 205433.
[52] L. Zhang, L. Y. Jiang, H. J. Yan, W. D. Wang, W. G. Song, Y. G. Guo, L. J. Wan, *J. Mater. Chem.* **2010**, *20*, 5462.
[53] D. Wei, Y. Liu, L. Cao, H. Zhang, Y. Wang, G. Yu, *Nano Lett.* **2009**, *9*, 1752.